remote sensing

MDPI

Article

Vegetation Effects on Soil Moisture Retrieval from Water Cloud Model Using PALSAR-2 for Oil Palm Trees

Veena Shashikant [1], Abdul Rashid Mohamed Shariff [1,2,3,*], Aimrun Wayayok [1,2,3], Md Rowshon Kamal [1], Yang Ping Lee [4] and Wataru Takeuchi [5]

1 Department of Biological and Agricultural Engineering, Faculty of Engineering, Universiti Putra Malaysia, Serdang 43400, Malaysia; gs52191@student.upm.edu.my (V.S.); aimrun@upm.edu.my (A.W.); rowshon@upm.edu.my (M.R.K.)
2 SMART Farming Technology Research Center, Faculty of Engineering, Universiti Putra Malaysia, Serdang 43400, Malaysia
3 Laboratory of Plantation System Technology and Mechanization (PSTM), Institute of Plantation Studies (IKP), Universiti Putra Malaysia, Serdang 43400, Malaysia
4 FGV R&D Sdn Bhd, Level 9, Wisma FGV, Jalan Raja Laut, Kuala Lumpur 50350, Malaysia; yangp.lee@fgvholdings.com
5 Department of Human and Social Systems, Institute of Industrial Science, The University of Tokyo, Tokyo 153-8505, Japan; wataru@iis.u-tokyo.ac.jp
* Correspondence: rashidpls@upm.edu.my; Tel.: +60-3-9769-6414

Abstract: In oil palm crop, soil fertility is less important than the physical soil characteristics. It is important to have a balance and sufficient soil moisture to sustain high yields in oil palm plantations. However, conventional methods of soil moisture determination are laborious and time-consuming with limited coverage and accuracy. In this research, we evaluated synthetic aperture radar (SAR) and in-situ observations at an oil palm plantation to determine SAR signal sensitivity to oil palm crop by means of water cloud model (WCM) inversion for retrieving soil moisture from L-band HH and HV polarized data. The effects of vegetation on backscattering coefficients were evaluated by comparing Leaf Area Index (LAI), Leaf Water Area Index (LWAI) and Normalized Plant Water Content (NPWC). The results showed that HV polarization effectively simulated backscatter coefficient as compared to HH polarization where the best fit was obtained by taking the LAI as a vegetation descriptor. The HV polarization with the LAI indicator was able to retrieve soil moisture content with an accuracy of at least 80%.

Keywords: SAR; backscattering; soil moisture content; LAI; HH and HV polarization

Citation: Shashikant, V.; Mohamed Shariff, A.R.; Wayayok, A.; Kamal, M.R.; Lee, Y.P.; Takeuchi, W. Vegetation Effects on Soil Moisture Retrieval from Water Cloud Model Using PALSAR-2 for Oil Palm Trees. *Remote Sens.* **2021**, *13*, 4023. https://doi.org/10.3390/rs13204023

Academic Editors: Takeo Tadono and Masato Ohki

Received: 31 August 2021
Accepted: 5 October 2021
Published: 9 October 2021

1. Introduction

Soil moisture content is a critical input variable in a wide variety of scientific studies in the field of agriculture. Soil moisture is an environmental element that connects the Earth's surface and the atmosphere. When soil moisture levels are balanced, agricultural yields improve, yield losses due to drought are reduced, and groundwater levels are recharged, ensuring the continuity of rivers and stream flows [1]. Oil palm trees require a reasonably steady high temperature, and continuous precipitation all year. Furthermore, prolonged dry periods of more than 2–3 months do not directly harm vegetative growth but have a significant impact on the yield and quality of fruit bunches [2]. The yield of oil palm is highly dependent on the availability of water during the sex differentiation of its inflorescences, which occurs approximately 28 months before bunch harvest. Soil moisture is therefore critical for optimal production in the oil palm crop [3]. Plants may be stressed if there is a water shortage. When water is not a constraint, potential evapotranspiration is the quantity of water that might be evaporated or transpired at a given temperature and humidity [4]. Water is a key component of plant tissue and is used to transport metabolites and minerals inside the plant. Water is also required for cell expansion, whereby it increases

the turgor pressure [5]. Many of the physiological processes related to growth are harmed by water deficiency in the soil, and severe deficiency may even result in the death of the plant. The effect of water deficiency, on the other hand, varies depending on the degree and length of water stress as well as the oil palm's development stage [6]. Nitrogen, Potassium, Magnesium, Boron, Copper, and Zinc are said to be essential nutrient components in oil palm crop soil for maximum growth [7]. The soil system and its activities are governed by nutrient availability, which leads to greater drought, insect, pest, and disease resistance [8]. Moreover, oil palm fronds have a delicate water transport system, which may expose them to increasing drought stress when the environment heats and dries [9]. Soil fertility refers to the soil's ability to deliver nutrients to the palm, including water availability for nutrient absorption and yield where soil–water conservation is carried out commonly to prevent soil erosion beneath mature palms, build terracing and silt pits in steep areas, mulch with empty fruit bunches and trunk chips, and cultivate leguminous cover crops [10]. Therefore, effective water management is the key to achieving high oil palm yield. As a result, sufficient soil moisture in the root zones is required, as too little or too much of it would reduce oil palm yields [11]. Recently, it was found that oil palm crop demands range from 0.893 to 1.6 million cubic meters; where ultimately, the actual requirement is site-specific and varies based on the soil moisture deficit, root zone water availability, and rooting depth [12].

Soil moisture has traditionally been measured directly at sampling places using gravimetry, which is a highly reliable and therefore often preferred method [13]. The results from gravimetric methods, however, only reflect a very limited region that changes instantly as the sampled field changes around the sampling site [14]. Remote sensing, both active and passive, enables unique studies of soil moisture at multiple spatial scales; therefore addressing agricultural scientific and application demands [15–17]. In passive remote sensing, Google Earth-based imageries and Normalised Difference Vegetation Index (NDVI) were used to determine the effect of land use and change of water storage in an oil palm plantation by measuring variations in soil water content over time [18]. Plus, the use of the NDVI and the Soil Adjusted Vegetation Index (SAVI) in oil palm crop to determine plant health by adopting a regression model technique revealed a highly correlated relationship between plant health based on NDVI analysis and nitrogen content to SAVI [19]. Additionally, to overcome the lack of soil information for farmers, a real-time palm oil soil monitoring system was built for Palm Oil Soil Monitoring in a Smart Agriculture where it can process, transmit, display, and conclude the soil's state via smartphone [20].

On the other hand, active remote sensing or SAR sensors are mostly used to assess soil moisture and crop water usage over broad regions [21]. SAR sensors are capable of identifying the spatial pattern of volumetric soil moisture due to their ability to penetrate to a depth of approximately 5 cm below the surface [22]. The depth to which microwaves penetrate, on the other hand, is mostly controlled by the density of vegetation, the stage of crop development, and sensor-related factors such as incidence angle, polarization, and frequency [23]. Recently, SAR sensor usage has increased over time, especially when the soil dielectric constant shows a linear relationship to the backscatter coefficient in the unit of decibels [24]. The microwave signals from the HH polarization often penetrate efficiently in the vegetation while reducing the interactions resulting from trunk or branches when compared to VV polarization [25]. When the sensor incidence angle was studied, the higher incident angles provided a better penetration as well as higher accuracy for soil moisture retrieval for both HH and VV [26]. Additionally, longer wavelengths or L-bands provide an adequate level of soil moisture sensitivity beneath the majority of plant cover [27,28]. In oil palm crop, AIRSAR backscattering coefficients were found to initially increase with age and the oil palm biomass is mentioned to be highly correlated at r = 0.85; where a Gamma filter of 11 × 11 window discriminates oil palm age classes effectively [29]. Following that, using the backscatter coefficient of fully polarized ALOS PALSAR data, biomass estimations were generated for an oil palm plantation in Malaysia and higher correlations were achieved

from VH polarization data [30]. Similarly, the biomass estimation of oil palm plantations using a regression analysis of HV polarized PALSAR was carried out [31].

A few SAR backscatter modelling techniques have been carried out to explore the influence of surface-related variables on the backscatter coefficient, such as topography and vegetation. These models are generally divided into theoretical, semi-empirical and empirical methods. Theoretical techniques such as the Integral Equation Model (IEM) and advanced IEM are complex, where the main challenge in assembling model parameters that accurately characterize the canopy is tough [32] as it requires a large number of parameters [33,34]. In addition to that, the empirical methods, for example the Dubois model [35], are simpler than the IEM models. However, the Dubois model has been reported to be dependent on experimental site and data conditions [36], where the saturation points were reported at lower NDVI values [37].

When the semi-empirical method was used, effects of vegetation cover using the WCM [38] were initially developed and later on were modified [39–41]. WCM is preferred for its simplicity [42] where it defines the overall backscatter coefficient obtained by the sensor over vegetated surfaces as the incoherent sum of the effects of vegetation and soil [43]. In this model, the canopy is often represented as a set of exact variables such as plant density per area, leaf size and orientation, which complicates and makes the model hard to interpret [44]. Many factors influence the backscatter coefficients from vegetation canopies, e.g., size of disperses in a canopy; the shape of scatters in a canopy; the orientation in a canopy; and the geometry of the canopy cover on ground [32]. To begin with, the WCM was modelled using plant height and water content of the vegetation layer to allow for the retrieval of soil moisture [38], and Leaf Area Index (LAI) was subsequently evaluated [45]. Other vegetation descriptors in the WCM were used from various combinations such as leaf water area index (LWAI), Normalized Plant Water Content (NPWC), vegetation water mass, and biomass [43,46–48].

The goal of this research is to optimize soil moisture retrieval using the WCM, thereby reducing the effect of vegetation on the crop-covered soil moisture backscatter coefficient. The WCM attempts to express vegetation cover scattering and attenuation terms in the concept through plain vegetation descriptors. Furthermore, a comparison analysis is performed on the use of the three primary vegetation descriptors, LAI, NPWC, and LWAI, singly or in combination, in the retrieval of soil moisture from PALSAR-2 data from Malaysian oil palm trees.

2. Materials and Methods

To recover soil moisture, a basic WCM was used in this investigation. Assuming that the effect of soil surface roughness on observed backscatter is consistent over a short time period for a given site, the temporal change in SAR backscattering only reflects changes in vegetation and soil moisture [49]. As a result, for this investigation, multi-temporal SAR data were used in the WCM. The vegetation descriptors and actual soil moisture were determined using field collected data. The Root Mean Square Error (RMSE) and mean absolute error coefficient were utilized to analyze the soil moisture retrieval accuracy. The next sections describe WCM, vegetation descriptors used in the model and evaluation of data processing methods.

2.1. Water Cloud Model (WCM)

WCM was developed assuming that the canopy "cloud" contains identical water droplets randomly distributed within the canopy [38]. In a water cloud model, the expression developed incorporated the soil moisture and the vegetation parameters in the equation. WCM for a given polarization (pp) is given as

$$\sigma^{\circ}{}_{tot,pp} = \sigma^{\circ}{}_{veg,pp} + \sigma^{\circ}{}_{soil+veg,\ pp} + \tau^{2}{}_{pp}\sigma^{\circ}{}_{soil,pp} \quad (1)$$

where $\sigma^{\circ}{}_{tot,pp}$ is the total backscatter coefficient, $\sigma^{\circ}{}_{veg,pp}$ is the backscatter contribution of the vegetation cover, $\sigma^{\circ}{}_{soil+veg,\ pp}$ is the multiple scattering involving vegetation elements

and the soil surface, $\sigma^{\circ}{}_{soil,pp}$ is the backscatter contribution of the soil surface and $\tau^2{}_{pp}$ is the two-way vegetation attenuation. The second component in Equation (1) reflects the interaction of incident radiation with the underlying soil. Because the interaction is not a dominant factor in co-polarized radiation, it may be ignored [43,50]. Subsequent to the model development, there were studies that modified the mentioned model [45]. WCM, Equation (2) [43], with four empirical coefficients, A_{pp}, B_{pp}, C_{pp}, and D_{pp} where A_{pp} and B_{pp} are vegetative characteristics and C_{pp} and D_{pp} are soil parameters, was presented for the given polarization where pp is either HH or HV polarization. The parameter A_{pp} corresponds to the albedo of the vegetation, and B_{pp} is an attenuation factor seen in (3) and (4). The parameter D_{pp} indicates the sensitivity of the radar signal to soil moisture, and C_{pp} can be considered as a calibration constant in (5). Hence, the equation written for the given polarization where pp is HH and HV is modified to

$$\sigma^{\circ}{}_{tot,pp} = \sigma^{\circ}{}_{veg,pp} + \tau^2{}_{pp}\sigma^{\circ}{}_{soil,pp} \tag{2}$$

where

$$\sigma^{\circ}{}_{veg,pp} = A_{pp} \times \mathrm{V}_1 \times \cos\theta\left(1 - \tau^2{}_{pp}\right) \tag{3}$$

$$\tau^2{}_{pp} = \left(\mathrm{Exp}\left(-2 \times B_{pp} \times \mathrm{V}_2 \times \sec\theta\right)\right) \tag{4}$$

V_1 and V_2 describe the effect of canopy water content and its geometry on backscatter coefficients. Vegetation descriptors have different effects on the WCM model. Therefore, several experimental studies on different combination of vegetation variables to quantify V_1 and V_2 in WCM were conducted by using plant height, LAI, LWAI and NPWC [51]. In Equations (3) and (4), θ is the incident angle of the image used, A_{pp} and B_{pp} are the vegetation parameter. M_v is the volumetric soil moisture and C_{pp} and D_{pp} are the soil parameter in Equation (5).

$$\sigma^{\circ}{}_{soil,pp} = D_{pp}M_v + C_{pp} \tag{5}$$

In this study, the LAI of palm fronds is defined by the amount of leaflet surface area per unit ground area [3]. LWAI is a product of LAI of palm fronds multiplied by the amount of water (W), expressed as the ratio of the difference between wet and dry mass to wet mass as in Equations (6) and (7).

$$LWAI = (LAI \times W) \tag{6}$$

$$W = \left(\frac{m_w - m_d}{m_w}\right) \tag{7}$$

where m_w and m_d are field records for freshly plucked and oven-dried mass of vegetation samples, respectively. Normalised plant water content, NPWC, also plays a dominant part in attenuating backscatter [38]. NPWC is like Equation (8) but divided with dry mass instead of wet mass.

$$NPWC = \left(\frac{m_w - m_d}{m_d}\right) \tag{8}$$

In this study, 5 combinations were used to understand the vegetation effects of WCM by using

Case 1 where V_1 = 1 and V_2 = LAI
Case 2 where V_1 = LAI and V_2 = 1
Case 3 where V_1 = LAI and V_2 = LAI
Case 4 where V_1 = LWAI and V_2 = LWAI
Case 5 where V_1 = NPWC and V_2 = NPWC

2.2. Estimating Parameters of A, B, C and D in the WCM

The estimation of parameters C_{pp} and D_{pp} are solved using a linear model fitting, following which, the values of C_{pp} and D_{pp} are substituted into Equation (2), which

allows for parameter A_{pp} and B_{pp} to be solved using the Nonlinear Least Squares Method (NLSM) [51–54]. It was noted that using Levenberg–Marquardt (LM) optimization in NLSM, an estimation of A_{pp} and B_{pp} can be made [55]. According to the optimization, LM is a common approach for addressing nonlinear least square issues that emerge from fitting a parameterized function to a collection of observed data points by minimizing the sum of the squares of the errors between the observed data points and the function output [56]. The LM algorithm is an iterative process which combines the Gauss–Newton method and the gradient descent method [57].

2.3. Evaluating WCM

To validate the WCM prior to inversing the model for accuracy and estimation performance metrics which include the coefficient of determination (R^2), the RMSE and the mean absolute error (MAE) were examined. The RMSE derived using Equation (9) was tested in most studies [49,55,57,58]. RMSE is a frequently used measure of the difference between values predicted by a model and the values observed from the environment that is being modelled. RMSE evaluation is given in Equation (9); X_{sim} is the simulated $\sigma^{\circ}{}_{tot,pp}$, X_{obs} is the observed $\sigma^{\circ}{}_{tot,pp}$ and n is the sample count. These individual differences are also called residuals, and the RMSE serves to aggregate them into a single measure of predictive power [59].

$$RMSE = \left(\sqrt{\frac{\sum_{i=1}^{n} (X_{sim} - X_{obs})^2}{n}} \right) \quad (9)$$

Together with R^2 and RMSE, the MAE was explored to further evaluate the model [60]. MAE is the average magnitude of the errors in a set of predictions, without considering their direction [61]. It is the average over the test sample of the absolute differences between prediction and actual observation where all individual differences have equal weight, as seen in (10)

$$MAE = \frac{1}{n} \sum_{i=1}^{n} |X_{sim} - X_{obs}| \quad (10)$$

3. Study Area and Datasets

3.1. Study Area

The study area of this research was in Chuping district, Perlis state, which comprises a region of flat-terrain oil palm cultivation. The area mentioned is about 28 ha. It covers 4 years of old palm stands which have just started fruiting. The center point coordinates of the study area are 6°31′07.2″ N 100°19′07.7″ E. In Chuping district, there are seven sub-districts namely Panggas, Sungai Buloh, Kubang Perun, Guar Nangka, Felda Chuping, Sungai Buloh, and Kilang Gula Chuping. This research took place at the Kilang Gula Chuping subdistrict as shown in Figure 1. The field data collected in this research were soil moisture, leaf moisture content, and leaf area index from frond 17 of the palms. Field data collection was planned to match the acquisition date of PALSAR-2 as shown in Section 3.2.

In the research site, the soil type was identified as Chuping and Dampar soil series, where the Chuping soil type is categorized as sandy clay loam with a hue of 7.5–10 YR (Yellow to Red) following the Munsell color chart standards, and the latter soil type was identified as clay loam with a hue of 7.5 YR [62]. The site was considered flat topography with an elevation of 21.6 m while the slope class was identified as 4–12% [63]. As per the study site, the months of February to March of the calendar year are regarded as the driest season of the year; with a maximum of 28 days of dry spell every year and an average of 1362.38 mm of precipitation per year in the years of 2015–2017 [64]. In the PALSAR-2 image acquisition months, Table 1 shows the monthly meteorological data obtained from Malaysian Meteorological Department. The observation dates in Table 1 represent the annual weather of the study area where the month of January was observed to be drier than April and July; however, the Mean Evaporation and Mean Radiation were similarly recorded.

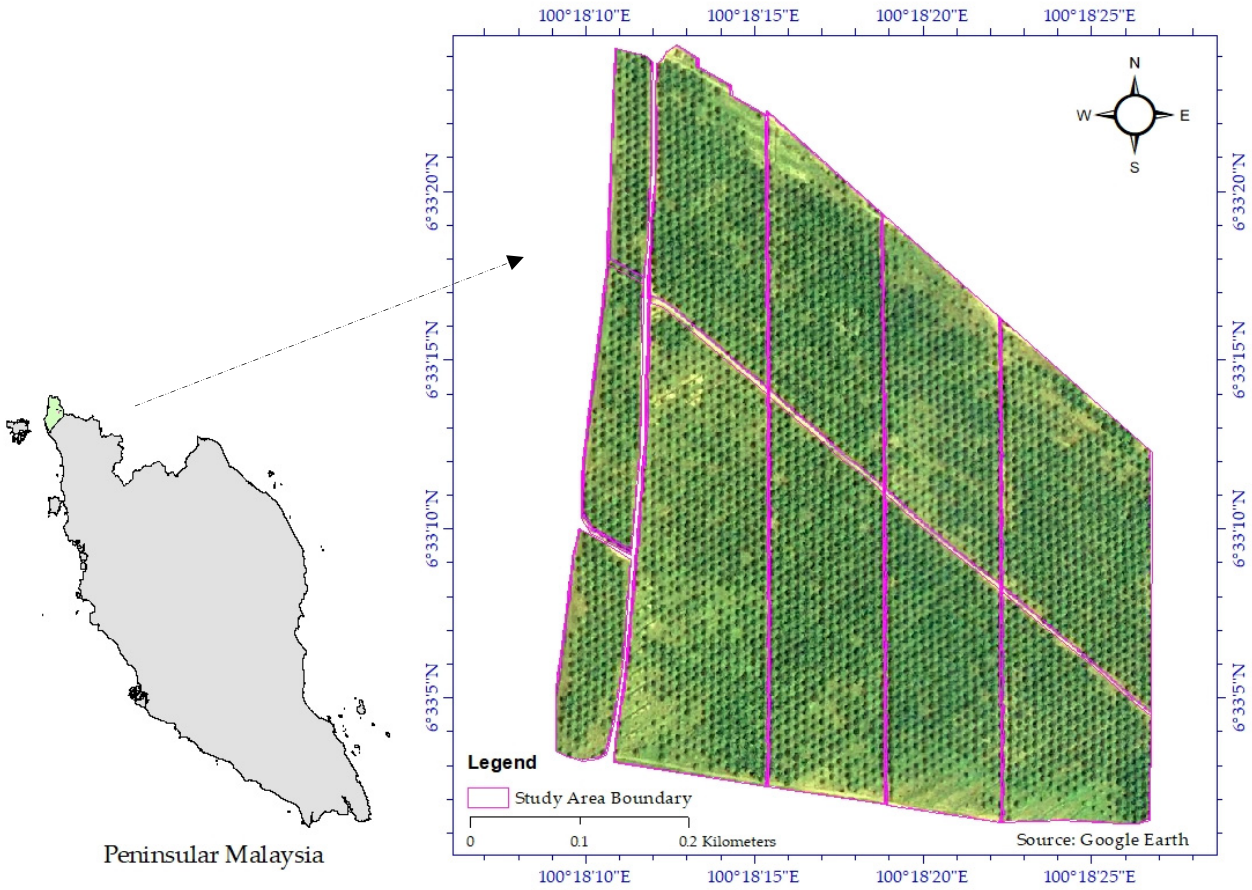

Figure 1. The oil palm cultivated area within the Chuping district in Perlis, Malaysia.

Table 1. Meteorological information of study area.

Month	Daily Meana Temperature (°C)	Total Precipitation for the Month (mm)	Daily Mean Radiation (MJm^{-2})	Daily Mean Evaporation (mm)
January	27.6	32.4	18.3	5.0
April	29.0	89.4	20.8	5.0
July	27.7	61.2	18.6	4.6

3.2. Data and Processing

PALSAR-2 signals were used for extracting the backscatter coefficient from the oil palm trees. High resolution scenes of PALSAR-2 were obtained under our collaboration with the Earth Observation Research Announcement 2 (EO-RA-2) of the Japanese Aerospace Exploration Agency (JAXA). We used a total of 3 PALSAR-2 scenes in this research, details of which are given in Table 2.

The acquired PALSAR-2 data were first converted from their Digital Number (DN) to backscatter coefficients in decibels, dB for both polarizations. Once the $\sigma^{\circ}{}_{HH}$ and $\sigma^{\circ}{}_{HV}$ for each of the field points was available, georeferencing of both images using SRTM (3 Sec) was done. The Lee filter was applied with a 5×5 window size to remove speckle and noise from the image. All the rectification process was completed in the SNAP open-source software. Additionally, Unmanned Aerial Vehicle (UAV) imagery was acquired on 17 January 2019 with the spatial resolution of 8 by 8 cm consisting of the red, blue, green, red edge and near infrared bands. The imagery from the UAV platform allowed us to compute the NDVI to identify bare soil areas in the field for the calibration process, with an NDVI value less than 0.2 taken to be bare soil. Ground truthing was done to validate the bare soil areas.

Table 2. Details of PALSAR-2 images.

Date of Acquisition	Flight Direction	Mode	Resolution	Polarization	Incident Angle
17 January 2019	Ascending	Strip Map 3	6.25 m × 6.25 m	HH + HV	30.4–42.4°
19 April 2019	Ascending	Strip Map 3	6.25 m × 6.25 m	HH + HV	41.2–53.3°
9 July 2019	Ascending	Strip Map 3	6.25 m × 6.25 m	HH + HV	30.4–42.4°

3.3. In-Situ Data Collection

The determination of soil moisture content at soil depth 0–5 cm was done using the soil gravimetric method. Fresh weight of soil moisture collected in field was recorded whereas the dry weight was determined after oven drying of the soil samples in the laboratory. A total of 32 points of soil sample were taken at each observation dated 17 January, 19 April and 9 July 2019, totalling to 96 soil samples altogether.

For the LAI for oil palm trees, a conventional method of destructive sampling was carried out using Equation (11). The frond to be chosen must not only be a good indicator of the nutrient status of the palm, but must also be one which is easy to identify and is consistent. By convention, frond 17 is used commonly in the oil palm fields. It is reported that frond 17 provides satisfactory results from its use as an input in the LAI formula [65]. According to the localised LAI formula, LAI was determined by the following equation:

$$LAI = \left(A_f \times F_n \times \frac{P_{DEN}}{10{,}000} \right) \mathrm{m}^2/\mathrm{m}^2 \tag{11}$$

where A_f is the leaf area per frond (m^2), F_n is the number of fronds per palm; P_{DEN} is the planting density where the number of palms per hectare is identified. Leaflets from the one-sided leaflet area were multiplied by two to obtain the total leaflet area of the frond in this research [66]. All leaflets were brought to the laboratory to determine the leaflet area using the LI-3100C, LI-COR Inc., which is USA-made equipment. Samples from the leaflets were taken and oven dried at 70 °C for 72 h until constant weight was achieved. An electronic balance was used to weigh the oven dried leaflets upon the completion of drying step. Similarly, the LWAI and NPWC were used from the same samples and methods as seen in Equations (6)–(8).

4. Results and Discussion

4.1. In-Situ Results

Field data collection for the three observation periods was based on the availability of PALSAR-2 orbit path data acquisition. In situ information was simultaneously collected for the soil moisture. LAI, LWAI and NPWC were calculated to understand the range values and average of each component in field. In Table 3, it can be noted that during the January and April data collection, the soil moisture average was 0.240 m^3/m^3 whereas the July data acquisition showed an increase in soil moisture recording at 0.273 m^3/m^3. Overall, for the palm trees cultivated areas, the soil moisture at the depths of 0–5 cm was averaged at 0.251 m^3/m^3. LAI for the palm fronds was averaged at 1.845 m^2/m^2 where it was seen to increase at every observation date, being 1.748, 1.784 and 2.005 m^2/m^2, respectively, during the January, April, and July observations dates. For the water content based on LAI in the palm fronds, an increase on each observation date was observed as well; the January observation date was at 0.205, 0.353 for the April observation date and 0.396 in the July observation date. This gave an average of 0.368 for all three observation dates. It can be noted that the study area faced drought stress in the earlier months of the calendar year where January to March recorded a lower rainfall [64]. Normalized plant water content was similar in all the observations at an average of 0.199%.

Table 3. Summary of in-situ data collection of Soil Moisture, LAI, LWAI and NPWC.

Observation Date	Soil Moisture (m^3/m^3)		LAI (m^2/m^2)		LWAI (% W in m^2/m^2)		NPWC (%)	
	Range	Mean	Range	Mean	Range	Mean	Range	Mean
17 January 2019	0.075–0.419	0.240	0.680–3.251	1.748	0.123–0.532	0.205	0.169–0.228	0.205
19 April 2019	0.170–0.316	0.240	0.662–3.174	1.784	0.125–0. 668	0.353	0.185–0.233	0.198
9 July 2019	0.119–0.454	0.273	1.214–3.078	2.005	0.076–0.661	0.396	0.052–0.221	0.195
Overall	0.075–0.454	0.251	0.661–3.251	1.845	0.076–0.668	0.368	0.052–0.233	0.199

4.2. Water Cloud Model Parameterization

The WCM model parameterization values were calibrated using bare soils and vegetation points from the NDVI values, derived from the RGB-NIR data obtained from UAV data acquisition, to fit the WCM model with the ground range values. Table 4 shows the vegetation parameters, A_{pp} and B_{pp} and the soil parameters C_{pp} and D_{pp} for the given polarization together with the combination indicator that represents the simulated scenarios of Cases 1–5. Using these vegetation and soil parameters together with LAI, LWAI, and NPWC as the input values, the WCM model was able to replicate the backscatter coefficients.

Table 4. WCM PALSAR-2 polarization calibration parameters for oil palm trees and combination vegetation descriptors used in this study.

Image Polarization	Combination Indicator	Vegetation Parameters		Soil Parameters	
		A_{pp}	B_{pp}	C_{pp}	D_{pp}
HH	Case 1	0.0118	0.0006	−26.0150	−2.8638
	Case 2	0.2188	0.0027	−26.0150	−2.8638
	Case 3	0.8467	0.0134	−26.0150	−2.8638
	Case 4	0.7122	0.0063	−26.0150	−2.8638
	Case 5	0.7457	0.0089	−26.0150	−2.8638
HV	Case 1	0.0850	0.0011	22.2070	−23.8660
	Case 2	0.1634	0.0047	22.2070	−23.8660
	Case 3	0.2530	0.0019	22.2070	−23.8660
	Case 4	0.4193	0.0321	22.2070	−23.8660
	Case 5	0.0182	0.0751	22.2070	−23.8660

4.3. Backscatter Simulation Based on the Proposed Vegetation Descriptors

Backscatter coefficients at frequency range of C and X bands are dominated by scattering activities in the crown layer of branches and foliage in the canopies, whereas scattering processes involving substantial trunks and branches would be dominated at lower frequencies like P and L bands [67]. In this study, the L band from PALSAR-2 was considered to give a better penetration in oil palm tree structure where backscatter coefficient characterizes the nature of oil palm structure. It was reported that oil palm trees using L band were capable to penetrate to the basal trunk in the oil palm plantation using both HH and HV polarizations [68]. Using the WCM model, the backscatter coefficients were simulated using a combination of vegetation descriptors. These simulated backscatter coefficients were then compared with the image-derived backscatter where the observed backscatter values were extracted from PALSAR-2. Table 5 shows the comparison of the backscatter coefficients observed and simulated for the study site. Both HH and HV polarizations showed a positive indication of a fitted WCM model using the respective vegetation descriptors where R^2 values ranged from 0.823 to 0.998, indicating the regression model fits the observed data well. In most HV polarization, the regression was found to be higher

than HH polarization using the WCM model. On the evaluation of the RMSE and MAE, it was found that the errors were minimized in the HV polarization.

Table 5. Metrics comparison between observed and simulated backscatter coefficients from WCM for HH and HV polarization with respect to the vegetation descriptors.

Description (n = 96)	Case 1		Case 2		Case 3		Case 4		Case 5	
	HH	HV	HH	HV	HH	HV	HH	HV	HH	HV
R^2	0.962	0.997	0.956	0.965	0.823	0.998	0.919	0.995	0.969	0.951
RMSE (dB)	2.259	0.222	2.266	0.782	2.384	0.158	2.222	0.387	2.256	0.351
MAE	1.821	0.212	1.814	0.212	1.872	0.150	1.789	0.366	1.811	0.280

Using the LAI vegetation descriptor, the Case 3 where LAI was used in both V_1 and V_2, HV showed the highest R^2 value of 0.998 with a lowest RMSE of 0.158 dB, indicating an efficient estimation of simulated backscatter coefficient. In comparison, HH showed a lower R^2 value of 0.823. Based on the RMSE and MAE evaluation, HV recorded more accurate values of 0.158 dB and 0.150 for RMSE and MAE, respectively, when compared to HH polarization which had values of 2.384 dB and 1.872 for RMSE and MAE, respectively. In the Case 1 where V_1 = 1 and V_2 = LAI, the HV polarization was more efficient to the simulate the backscatter coefficient with RMSE 0.222 dB and R^2 = 0.997. However, the HH polarization, even though it shows good R^2 of 0.962, had higher RMSE with 2.259 dB. Using the LAI indicator as V_1 and V_2 as 1, both HH and HV polarizations showed a good R^2 with 0.956 and 0.965, respectively, but the RMSE was lower by 1.584 dB in the HV polarization. The MAE gave lower values for the HV polarization with 0.212. In Case 4 using LWAI, the model accurately predicted the simulated backscatter with R^2 = 0.995 in the HV with 0.387 dB RMSE and MAE of 0.366. When the NPWC vegetation descriptors was evaluated for HH polarization, its R^2 value of 0.969 was higher than the HV polarization R^2 of 0.951, but the MAE in HV polarization was computed to be lower than HH polarization by 1.531 and RMSE by 1.905 dB, which means the latter polarization is more accurately simulated. It is important to note that in the LAI combinations of the vegetation descriptors, dual use of LAI was found to be the most accurate parameter to simulate backscatter coefficient values. Furthermore, it is critical to produce an accurate simulation of the backscatter coefficient since it can convey the actual field range values obtained during the in-situ collection utilizing the model. This understanding is important to allow future work to be carried out with minimal calibration values and adopted into large areas of plantations where it is remotely challenging to access the collected field data and senses.

4.4. Vegetation Effects on Soil Moisture Retrieval Based on Polarization

Vegetation descriptors play an equally important role in the estimation of the backscatter coefficient as well as providing reliable information to showcase the ground parameters in the WCM model. The backscattering coefficient mechanism interaction with soil moisture is complex [69]. Recently, in an attempt to reduce complexity in the modified IEM, the soil parameters were being simplified from three to two soil parameters [70]. Earlier studies have demonstrated the necessity to eliminate the effects of vegetation on soil moisture retrieval [71]. It was discovered that soil moisture retrieval is much more accurate when vegetation cover is considered [72]. To further explore the backscatter coefficients derived in Section 4.3 with different vegetation descriptors, the soil moisture was retrieved from the backscatter to allow comparison of observed soil moisture in the oil palm study area. It was seen that the simulated backscatter coefficient was predicted from the ground soil moisture values accurately given the observation period variability of lesser rainfall in the January observation when compared to the other observations. By making comparisons with the soil moisture retrieved from PALSAR-2 images, the model can be cross-evaluated to see the model fitting using the WCM. The vegetation descriptors evaluated as mentioned by Cases 1–5 can be seen in Table 6. In this comparison between the retrieved and

observed soil moisture values, we have the best case with the highest R^2 value of 0.805 and the lowest RMSE of 0.046 m^3/m^3. When looking at Case 1 for HV polarization, the soil moisture retrieved was plotted against simulated backscatter coefficient where the R^2 was demonstrated at 0.916, as seen in Figure 2. Similar accuracy was achieved using Radarsat-2 utilizing the LAI descriptor, whereby RMSE of 0.069 m^3/m^3 was reported [73]. The initial combination introduced in the WCM [38], with V_1 as 1 and V_2 as LAI providing the most promising soil moisture retrieval in the oil palm trees in this study, as seen in Figure 2. LAI parameter was evaluated as one of the best parameters when VV polarization was compared to LWAI and NPWC, with 4.19–4.43% of the RMSE [51]. Signal backscattering is influenced by canopy structure where it is very sensitive to plant water content, a variable highly correlated with LAI during the vegetative phase [74].

Table 6. Comparison between statistical parameters of retrieved and observed soil moisture for HH and HV polarization in relation to the vegetation descriptors.

Image Polarization	Description (n = 96)	Case 1	Case 2	Case 3	Case 4	Case 5
HH	R^2	0.598	0.512	0.490	0.727	0.558
	RMSE (m^3/m^3)	0.088	0.091	0.101	0.085	0.089
	MAE	0.070	0.072	0.080	0.069	0.071
HV	R^2	0.805	0.609	0.675	0.459	0.301
	RMSE (m^3/m^3)	0.046	0.057	0.051	0.066	0.075
	MAE	0.043	0.047	0.044	0.050	0.058

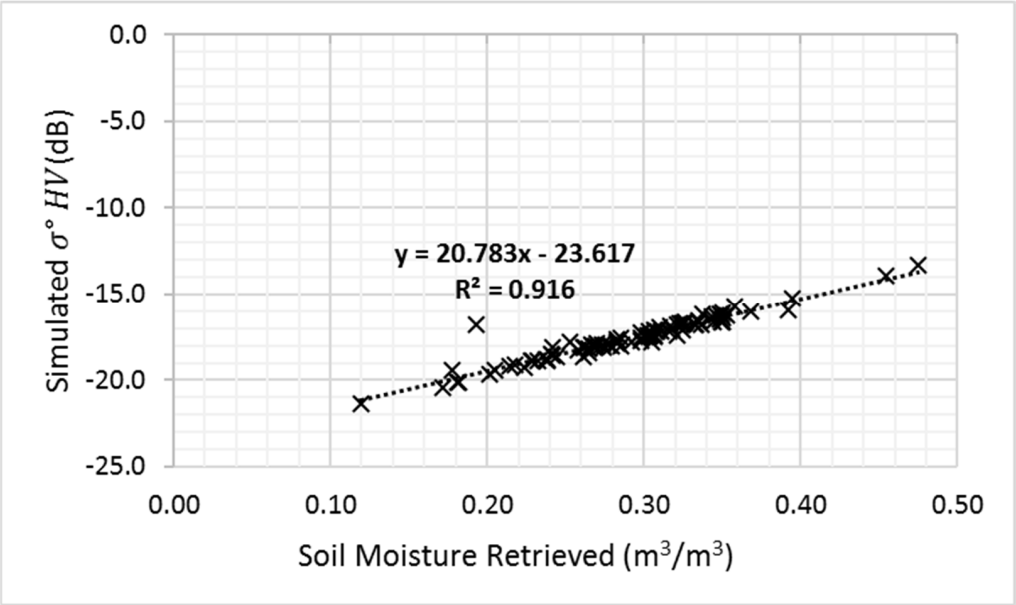

Figure 2. Soil moisture retrieved using vegetation descriptors of V_1 = 1 and V_2 = LAI, and simulated backscatter coefficient of HV polarization.

It can be observed that the Case 4 using LWAI as vegetation descriptors, using HH polarization gave an R^2 value of 0.727 where the RMSE was found to be 0.085 m^3/m^3, the HV polarization recorded a lower error with an RMSE value of 0.066 m^3/m^3 with R^2 value of 0.727. In contrast, the lowest R^2 value of 0.301 was from the NPWC case where RMSE was observed at 0.075 m^3/m^3. Figure 3 shows the observed soil moisture based on polarization of PALSAR images. It can be noted that the HV polarization gives better lower RMSE values as compared to HH polarization, considering all the vegetation descriptors [75]. It was reported that HH polarization could provide a low RMSE value of 0.049 m^3/m^3 [71] using remote sensing-based vegetation descriptors, in this case Normalized Difference Infrared Index (NDII). Similarly, when canopy water content based on LAI was applied as a vegetation descriptor, an RMSE of 0.039 was recorded [53]. Overall, when RMSE and

MAE are carefully evaluated, the cross-polarized HV backscatter coefficient is revealed to be more vulnerable than the co-polarized backscatter HH in terms of polarization response in all Cases 1–5 observed.

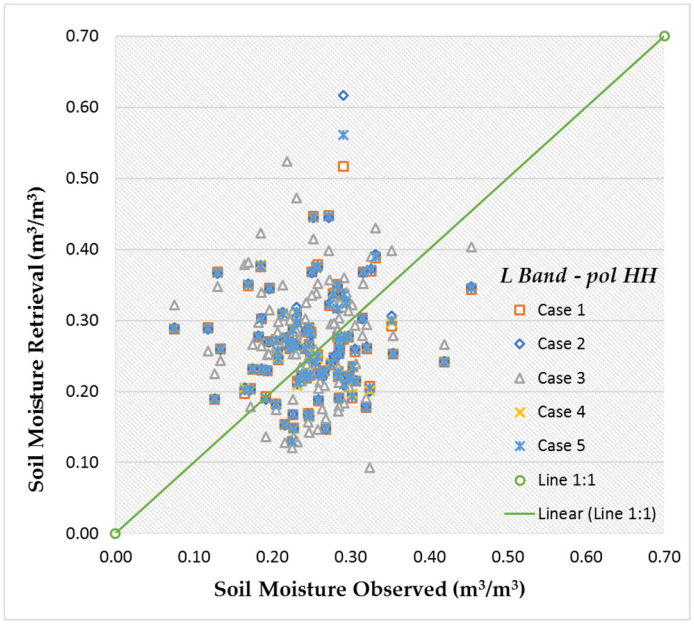

(**a**)

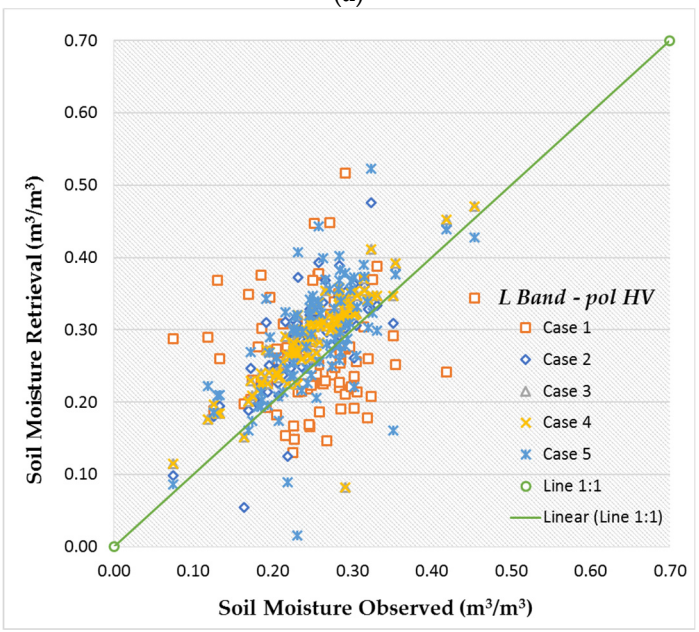

(**b**)

Figure 3. Observed soil moisture compared to retrieved soil moisture: Polarization in L band using (**a**) HH polarization and (**b**) HV polarization.

Our research results need to be interpreted with respect to the age of the oil palm stands which were 4 years old and our terrain type, whereby the terrain in our study was considered flat and the backscatter intensity represented in the acquired images was a composition of interactions with the crown, the trunk, and the ground surface of the current palm stands. However, it is known that oil palm crop growth or biomass increases over years, hence it is recommended that larger data sets need to be collected from the field to represent greater diversity of palm ages, possibly using fully polarimetric SAR data. Specifically, an understanding of the effects of backscattering on undulating grounds

and peatlands in oil palm growing areas will be helpful in future. This could help in understanding the influence of SAR on other variables of importance to the oil palm industry, such as estimation of vegetation water content of oil palm canopy and yield. Benefits of this research can be useful for the plantation industry especially with the increase in available high-resolution multi-polarization satellite SAR sensors. This allows for the possibilities in exploiting the use of oil palm crop-related parameters supported with satellite data input to a decision-making platform for oil palm plantations.

5. Conclusions

In this study, L band from PALSAR-2 observations and in-situ data collected were used to evaluate a WCM model for soil moisture retrieval in oil palm cultivated regions. The WCM was calibrated using NDVI values, then fitted to a WCM model by different instances of vegetation descriptors to evaluate the best fit for the model. Using the WCM model and LAI specifically as V_1 and V_2, it was found to provide the best simulated backscatter coefficient in the HV polarization, secondly followed by V_1 which is set as constant with a value of 1 and V_2 as LAI. For HV polarization, LAI specifically as V_1 and V_2 showed an R^2 of 0.998 in simulating the backscatter coefficient accurately with RMSE of 0.158 dB, whereas HH polarization showed a lower R^2 of 0.823 with a higher RMSE of 2.384 dB. However, when LWAI and NPWC were considered, the model fitted better with co-polarized backscatter, where HH backscatter coefficient records R^2 of 0.727 and 0.558, respectively. It can be said that the co-polarized backscatters have shown lower RMSE values in the model fit for all cases where it can be predicted to be more useful in retrieving soil moisture in oil palm cultivated areas. In this respect, this research makes a useful and novel contribution on soil moisture for the benefit of the oil palm cultivation, and we found the PALSAR-2 sensor data beneficial for this purpose. The findings of this research will eventually help the oil palm growers to have systems in place to address the abrupt droughts brought about by climate change. Future work of this research can be explored with SAR-based vegetation descriptors, e.g., Radar Vegetation Index and optical derived indices such as NDVI, Normalised Difference Water Index and NDII.

Author Contributions: Conceptualization, V.S. and A.R.M.S.; Data curation, V.S.; Formal analysis, V.S.; Investigation, A.R.M.S.; Methodology, V.S., A.R.M.S., M.R.K., Y.P.L. and W.T.; Resources, A.R.M.S., A.W., M.R.K., Y.P.L. and W.T.; Software, V.S.; Supervision, A.R.M.S. and A.W.; Validation, V.S., A.R.M.S., M.R.K., Y.P.L. and W.T.; Visualization, A.R.M.S. and A.W.; Writing—original draft, V.S.; Writing—review and editing, V.S., A.R.M.S., A.W., M.R.K., Y.P.L. and W.T. All authors have read and agreed to the published version of the manuscript.

Funding: This research was funded by the Japanese Aerospace Agency (JAXA), using the Earth Observation-Research Announcement (EO-RA2) collaboration with PI number of ER2A2N180 to obtained PALSAR-2 data.

Data Availability Statement: PALSAR-2 data was requested via proposal where restrictions apply for high resolution data.

Acknowledgments: The authors would like to thank Rajah Selvarajah for providing financial support for purchasing UAV data and field work logistics to complete the research work. The authors would like to express their gratitude to the Soil and Water Conservation Laboratory, Department of Biological and Agricultural Engineering, Faculty of Engineering, University Putra Malaysia (UPM), particularly Mohamad Hafis bin Ramli, for assistance with soil-related matters, particularly providing equipment for extracting soil samples and oven drying lab equipment. The authors would also like to express their gratitude to Ghazali bin Kassim, who arranged for GPS equipment from the Spatial Information System Laboratory, Biological and Agricultural Engineering, Faculty of Engineering, UPM, to be utilized for locating soil samples points in the field. Authors would like to thank the FGV R&D Sdn. Bhd. to support in-field arrangement leading to a smooth data collection especially to Mohd Shahkhirat bin Norizan, Syahidah Abu Hassan, Mazuan, Haryati Abidin, Noorsusilawati bt. Mandangan, Mohd Mahfuz Roslan, Muhammad Farid Abdul Rahim and Mohd Na'aim bin Samad.

Conflicts of Interest: The authors declare no conflict of interest in the process of writing this paper locally and internationally.

References

1. Benites, J.; Castellanos, A. Improving soil moisture with conservation agriculture. *Leisa Mag.* **2003**, *19*, 6–7.
2. Verheye, W. Growth and production of oil palm. In *Encyclopedia of Life Support Systems (EOLSS)*; UNESCO-EOLSS Publishers: Oxford, UK, 2010.
3. Noor, M.R.M.; Harun, M.H. Water deficit and irrigation in oil palm: A review of recent studies and findings. *Oil Palm Bull.* **2004**, *49*, 1–6.
4. Abubaker, J. Irrigation scheduling for efficient water use in dry climates. Master's Thesis, Swedish University of Agricultural Sciences, Uppsala, Sweden, 2001; p. 47.
5. Fahad, S.; Bajwa, A.A.; Nazir, U.; Anjum, S.A.; Farooq, A.; Zohaib, A.; Sadia, S.; Nasim, W.; Adkins, S.; Saud, S.; et al. Crop Production under Drought and Heat Stress: Plant Responses and Management Options. *Front. Plant Sci.* **2017**, *8*, 1147. [CrossRef] [PubMed]
6. Cha-um, S.; Yamada, N.; Takabe, T.; Kirdmanee, C. Physiological features and growth characters of oil palm (*Elaeis guineensis* jacq.) in response to reduced water-deficit and rewatering. *Aust. J. Crop Sci.* **2013**, *7*, 432–439.
7. Ng, S.K. Nutrition and nutrient management of the oil palm. New thrust for the future perspective. In *Potassium for Sustainable Crop Production. International Symposium on Role of Potassium in India*; Potash Research Institute of India and International Potash Institute: New Delhi, India, 2002; pp. 415–429.
8. Sundram, S.; Angel, L.P.L.; Sirajuddin, S.A. Integrated balanced fertiliser management in soil health rejuvenation for a sustainable oil palm cultivation: A review. *J. Oil Palm Res.* **2019**, *31*, 348–363. [CrossRef]
9. Waite, P.-A.; Schuldt, B.; Link, R.M.; Breidenbach, N.; Triadiati, T.; Hennings, N.; Saad, A.; Leuschner, C. Soil moisture regime and palm height influence embolism resistance in oil palm. *Tree Physiol.* **2019**, *39*, 1696–1712. [CrossRef] [PubMed]
10. Haron, K.; Tarmizi, A.M. Techniques of Soil and Water Conservation and Nutrient Recycling in Oil Palm Plantations on Inland Soils. *Oil Palm Bull.* **2008**, *56*, 1–11.
11. May, C.Y. Malaysia: Economic transformation advances oil palm industry. *Am. Oil Chem. Soc.* **2012**, *23*, 536–542.
12. Adesiji, A.R.; Nik Daud, N.N.; Asogwa, E.O.; Jarumi, A.M.; Musa, H.H.; Adaudu, I.I. Irrigation and crop water requirement estimation for oil palms using soil moisture balance model in Peninsular Malaysia. *J. Agric. Food Eng.* **2020**, *3*, 1–8.
13. Teixeira, W.G.; Huwe, B.; Schroth, G.; Marques, J.D. Sampling and TDR probe insertion in the determination of the volumetric soil water content. *Revista Brasileira de Ciência do Solo* **2003**, *27*, 575–582. [CrossRef]
14. Cepuder, P.; Evett, S.; Heng, L.K.; Hignett, C.; Laurent, J.P.; Ruelle, P.; Moutonnet, P.; Nguyen, M.L. Field estimation of soil water content: A practical guide to methods, instrumentation, and sensor technology. *IAEA Vienna* **2008**, *30*, 24.
15. Sishodia, R.P.; Ray, R.L.; Singh, S.K. Applications of Remote Sensing in Precision Agriculture: A Review. *Remote Sens.* **2020**, *12*, 3136. [CrossRef]
16. Njoku, E.G.; Entekhabi, D. Passive microwave remote sensing of soil moisture. *J. Hydrol.* **1996**, *184*, 101–129. [CrossRef]
17. Schmugge, T.J.; Kustas, W.P.; Ritchie, J.C.; Jackson, T.J.; Rango, A. Remote sensing in hydrology. *Adv. Water Resour.* **2002**, *25*, 1367–1385. [CrossRef]
18. Rau, M.I. Remote Sensing Approaches to Observe the Significance of Landuse Change on Water Storage at Oil Palm Plantation in Kuala Langat South Forest Reserve, Malaysia. Master's Dissertation, University of Glasgow, Glasgow, UK, 2008.
19. Foong, A.; Sum, W.; Shukor, S.A.A. Oil Palm Plantation Monitoring from Satellite Image. *IOP Conf. Ser. Mate. Sci. Eng.* **2019**, *705*, 1–8.
20. Rawi, R.; Miit, U.K.L.; Hasnan, M.S.I.; Sajak, A.A.B. Palm Oil Soil Monitoring System for Smart Agriculture. *Int. J. Integr. Eng.* **2020**, *12*, 189–199. [CrossRef]
21. Palazzi, V.; Bonafoni, S.; Alimenti, F.; Mezzanotte, P.; Roselli, L. Feeding the World with Microwaves: How Remote and Wireless Sensing Can Help Precision Agriculture. *IEEE Microw. Mag.* **2019**, *20*, 72–86. [CrossRef]
22. Zhuo, L.; Han, D. Science Direct the relevance of soil moisture by remote sensing and hydrological modelling. *Procedia Eng.* **2016**, *154*, 1368–1375. [CrossRef]
23. Lakshmi, V. Remote Sensing of Soil Moisture. *ISRN Soil Sci.* **2013**, *2013*, 33. [CrossRef]
24. Petropoulos, G.P.; Ireland, G.; Barrett, B. Surface soil moisture retrievals from remote sensing: Current status, products & future trends. *Phys. Chem. Earth Parts A/B/C* **2015**, *83–84*, 36–56.
25. ABalenzano, A.; Mattia, F.; Satalino, G.; Davidson, M.W.J. Dense Temporal Series of C- and L-band SAR Data for Soil Moisture Retrieval Over Agricultural Crops. *IEEE J. Sel. Top. Appl. Earth Obs. Remote Sens.* **2011**, *4*, 439–450. [CrossRef]
26. Joseph, A.T.; Van der Velde, R.; O'Neill, P.E.; Lang, R.; Gish, T. Effects of corn on C- and L-band radar backscatter: A correction method for soil moisture retrieval. *Remote Sens. Environ.* **2010**, *114*, 2417–2430. [CrossRef]
27. Barrett, B.; Dwyer, E.; Whelan, P. Soil Moisture Retrieval from Active Spaceborne Microwave Observations: An Evaluation of Current Techniques. *Remote Sens.* **2009**, *1*, 210–242. [CrossRef]
28. Ottinger, M.; Kuenzer, C. Spaceborne L-Band Synthetic Aperture Radar Data for Geoscientific Analyses in Coastal Land Applications: A Review. *Remote Sens.* **2020**, *12*, 2228. [CrossRef]

29. Nordin, L.; Shahruddin, A.; Mariamni, H. Application of AIRSAR data to oil palm tree characterization. In Proceedings of the Asian Conference on Remote Sensing, Bangkok, Thailand, 7–9 August 2002; pp. 1–7.
30. Shashikant, V.; Shariff, A.R.M.; Nordin, L.; Pradhan, B. Estimation of above ground biomass of oil palm trees by PALSAR. In Proceedings of the CHUSER 2012—2012 IEEE Colloquium on Humanities, Science and Engineering, Kota Kinabalu, Malaysia, 3–4 December 2012; pp. 838–841.
31. Morel, A.C.; Saatchi, S.S.; Malhi, Y.; Berry, N.J.; Banin, L.; Burslem, D.; Nilus, R.; Ong, R.C. Estimating aboveground biomass in forest and oil palm plantation in Sabah, Malaysian Borneo using ALOS PALSAR data. *For. Ecol. Manag.* **2011**, *262*, 1786–1798. [CrossRef]
32. Bindlish, R.; Barros, A.P. Parameterization of vegetation backscatter in radar-based, soil moisture estimation. *Remote Sens. Environ.* **2001**, *76*, 130–137. [CrossRef]
33. Chen, K.; Wu, T.-D.; Tsang, L.; Li, Q.; Shi, J.; Fung, A. Emission of rough surfaces calculated by the integral equation method with comparison to three-dimensional moment method simulations. *IEEE Trans. Geosci. Remote Sens.* **2003**, *41*, 90–101. [CrossRef]
34. Fung, A.K.; Chen, K.S. Dependence of the surface backscattering coefficients on roughness, frequency and polarization states. *Int. J. Remote Sens.* **2007**, *13*, 1663–1680. [CrossRef]
35. Dubois, P.; Van Zyl, J.; Engman, T. Measuring soil moisture with imaging radars. *IEEE Trans. Geosci. Remote Sens.* **1995**, *33*, 915–926. [CrossRef]
36. Gorrab, A.; Zribi, M.; Baghdadi, N.; Lili-Chabaane, Z.; Mougenot, B. Multi-frequency analysis of soil moisture vertical heterogeneity effect on radar backscatter. In Proceedings of the International Conference on Advanced Technologies for Signal and Image Processing (ATSIP), Sousse, Tunisia, 17–19 March 2014; pp. 379–384.
37. Dobson, M.C.; Ulaby, F.T.; Pierce, L.E.; Sharik, T.L.; Bergen, K.M.; Kellndorfer, J.; Kendra, J.R.; Li, E.; Lin, Y.C.; Nashashibi, A.; et al. Estimation of forest biophysical characteristics in Northern Michigan with SIR-C/X-SAR. *IEEE Trans. Geosci. Remote Sens.* **1995**, *33*, 877–895. [CrossRef]
38. Attema, E.P.W.; Ulaby, F.T. Vegetation modeled as a water cloud. *Radio Sci.* **1978**, *13*, 357–364. [CrossRef]
39. Ulaby, F.T.; Stiles, W.H.; Abdelrazik, M. Snowcover Influence on Backscattering from Terrain. *IEEE Trans. Geosci. Remote Sens.* **1984**, *GE-22*, 126–133. [CrossRef]
40. Baghdadi, N.; King, C.; Chanzy, A.; Wigneron, J.P. An empirical calibration of the integral equation model based on SAR data, soil moisture and surface roughness measurement over bare soils. *Int. J. Remote Sens.* **2010**, *23*, 4325–4340. [CrossRef]
41. Moran, M.S.; Peters-Lidard, C.D.; Watts, J.M.; McElroy, S. Estimating soil moisture at the watershed scale with satellite-based radar and land surface models. *Can. J. Remote Sens.* **2014**, *30*, 805–826. [CrossRef]
42. Gherboudj, I.; Magagi, R.; Berg, A.A.; Toth, B. Soil moisture retrieval over agricultural fields from multi-polarized and multi-angular RADARSAT-2 SAR data. *Remote Sens. Environ.* **2011**, *115*, 33–43. [CrossRef]
43. Prévot, L.; Champion, I.; Guyot, G. Estimating surface soil moisture and leaf area index of a wheat canopy using a dual-frequency (C and X bands) scatterometer. *Remote Sens. Environ.* **1993**, *46*, 331–339. [CrossRef]
44. Lang, R.H.; Saleh, H.A. Microwave Inversion of Leaf Area and Inclination Angle Distributions from Backscattered Data. *IEEE Trans. Geosci. Remote Sens.* **1985**, *GE-23*, 685–694. [CrossRef]
45. Ulaby, F.; Allen, C.; Eger, G.; Kanemasu, E. Relating the microwave backscattering coefficient to leaf area index. *Remote Sens. Environ.* **1984**, *14*, 113–133. [CrossRef]
46. Xu, H.; Steven, M.D.; Jaggard, K.W. Monitoring leaf area of sugar beet using ERS-1 SAR data. *Int. J. Remote Sens.* **2007**, *17*, 3401–3410. [CrossRef]
47. Dabrowska-Zielinska, K.; Inoue, Y.; Kowalik, W.; Gruszczynska, M. Inferring the effect of plant and soil variables on C- and L-band SAR backscatter over agricultural fields, based on model analysis. *Adv. Space Res.* **2007**, *39*, 139–148. [CrossRef]
48. Chauhan, S.; Srivastava, H.S.; Patel, P. Wheat crop biophysical parameters retrieval using hybrid-polarized RISAT-1 SAR data. *Remote Sens. Environ.* **2018**, *216*, 28–43. [CrossRef]
49. Li, J.; Wang, S. Using SAR-Derived Vegetation Descriptors in a Water Cloud Model to Improve Soil Moisture Retrieval. *Remote Sens.* **2018**, *10*, 1370. [CrossRef]
50. Ulaby, F.T.; Moore, R.K.; Fung, A.K. Microwave Remote Sensing. Active and Passive. From Theory to Applications. *Geol. Mag.* **1986**, *124*, 88.
51. Kumar, K.; Rao, H.P.S.; Arora, M.K. Study of water cloud model vegetation descriptors in estimating soil moisture in Solani catchment. *Hydrol. Process.* **2014**, *29*, 2137–2148. [CrossRef]
52. Khabazan, S.; Hosseini, M.; Saradjian, M.R.; Motagh, M.; Magagi, R. Accuracy Assessment of IWCM Soil Moisture Estimation Model in Different Frequency and Polarization Bands. *J. Indian Soc. Remote Sens.* **2015**, *43*, 859–865. [CrossRef]
53. Tao, L.; Wang, G.; Chen, X.; Li, J.; Cai, Q. Estimation of soil moisture using a vegetation scattering model in wheat fields. *J. Appl. Remote Sens.* **2019**, *13*, 044503. [CrossRef]
54. Zribi, M.; Baghdadi, N.; Bousbih, S.; El-Hajj, M.; Gao, Q.; Escorihuela, M.J.; Muddu, S. Soil Surface Moisture Estimation Using the Synergy S1/S2 Data. In Proceedings of the IGARSS 2018—2018 IEEE International Geoscience and Remote Sensing Symposium, Valencia, Spain, 22–27 July 2018; pp. 6119–6122.
55. Chauhan, S.; Srivastava, H.S.; Patel, P. Improved Parameterization of Water Cloud Model for Hybrid-Polarized Backscatter Simulation Using Interaction Factor. *ISPRS Int. Arch. Photogramm. Remote Sens. Spat. Inf. Sci.* **2017**, *XLII-4/W2*, 61–66. [CrossRef]

56. Gavin, H.P. *The Levenberg-Marquardt Algorithm for Nonlinear Least Squares Curve-Fitting Problems*; Department of Civil and Environmental Engineering, Duke University: Durham, NC, USA, 2020.
57. Mandal, D.; Kumar, V.; McNairn, H.; Bhattacharya, A.; Rao, Y. Joint estimation of Plant Area Index (PAI) and wet biomass in wheat and soybean from C-band polarimetric SAR data. *Int. J. Appl. Earth Obs. Geoinf.* **2019**, *79*, 24–34. [CrossRef]
58. Yadav, V.P.; Prasad, R.; Bala, R. Leaf area index estimation of wheat crop using modified water cloud model from the time-series SAR and optical satellite data. *Geocarto Int.* **2019**, *36*, 791–802. [CrossRef]
59. Irizarry, R.A. *Introduction to Data Science: Data Analysis and Prediction Algorithms with R*; CRC Press: Boca Raton, FL, USA, 2019.
60. Schönbrodt-Stitt, S.; Ahmadian, N.; Kurtenbach, M.; Conrad, C.; Romano, N.; Bogena, H.R.; Vereecken, H.; Nasta, P. Statistical Exploration of SENTINEL-1 Data, Terrain Parameters, and in-situ Data for Estimating the Near-Surface Soil Moisture in a Mediterranean Agroecosystem. *Front. Water* **2021**, *3*, 75. [CrossRef]
61. Hair, J.F.; Tomas, G.; Hult, M.; Ringle, C.M.; Sarstedt, M. *A Primer on Partial Least Squares Structural Equation Modeling (PLS-SEM)*, 3rd ed.; SAGE Publications: London, UK, 2021.
62. National Geospatial Centre. *Malaysian Standard Geographic Information/Geomatics Features and Attribute Codes*; Ministry of Energy and Natural Resources (KeTSA): Putrajaya, Malaysia, 2020.
63. Norizan, M.S.; Wayayok, A.; Karim, Y.A.; Abdullah, A.F.; Mahadi, M.R. Quantitative approach for irrigation requirement of oil palm: Case study in Chuping, Northern Malaysia. *J. Oil Palm Res.* **2021**, *33*, 278–288. [CrossRef]
64. Shashikant, V.; Mohamed Shariff, A.R.; Wayayok, A.; Kamal, M.R.; Lee, Y.P.; Takeuchi, W. Utilizing TVDI and NDWI to Classify Severity of Agricultural Drought in Chuping, Malaysia. *Agronomy* **2021**, *11*, 1243. [CrossRef]
65. Kok, Z.H.; Mohamed Shariff, A.R.; Khairunniza-Bejo, S.; Kim, H.-T.; Ahamed, T.; Cheah, S.S.; Wahid, S.A.A. Plot-Based Classification of Macronutrient Levels in Oil Palm Trees with Landsat-8 Images and Machine Learning. *Remote Sens.* **2021**, *13*, 2029. [CrossRef]
66. Awal, M.; Ishak, W.W. Measurement of Oil Palm LAI by Manual and LAI-2000 Method. *Asian J. Sci. Res.* **2007**, *1*, 49–56. [CrossRef]
67. Imhoff, M.L. Radar backscatter and biomass saturation: Ramifications for global biomass inventory. *IEEE Trans. Geosci. Remote Sens.* **1995**, *33*, 511–518. [CrossRef]
68. Hashim, I.; Mohamed Shariff, A.R.; Bejo, S.; Muharam, F.; Ahmad, K. Machine-Learning Approach Using SAR Data for the Classification of Oil Palm Trees That Are Non-Infected and Infected with the Basal Stem Rot Disease. *Agronomy* **2021**, *11*, 532. [CrossRef]
69. Jiang, N.; Xu, T.; Xu, Y.; Xu, G.; Schuh, H. Assessment of Different Stochastic Models for Inter-System Bias between GPS and BDS. *Remote Sens.* **2019**, *11*, 989. [CrossRef]
70. Baghdadi, N.; Zribi, M.; Paloscia, S.; Verhoest, N.E.C.; Lievens, H.; Baup, F.; Mattia, F. Semi-Empirical Calibration of the Integral Equation Model for Co-Polarized L-Band Backscattering. *Remote Sens.* **2015**, *7*, 13626–13640. [CrossRef]
71. Zhang, L.; Meng, Q.; Yao, S.; Wang, Q.; Zeng, J.; Zhao, S.; Ma, J. Soil Moisture Retrieval from the Chinese GF-3 Satellite and Optical Data over Agricultural Fields. *Sensors* **2018**, *18*, 2675. [CrossRef]
72. Kirimi, F.; Kuria, D.N.; Thonfeld, F.; Amler, E.; Mubea, K.; Misana, S.; Menz, G. Influence of Vegetation Cover on the Oh Soil Moisture Retrieval Model: A Case Study of the Malinda Wetland, Tanzania. *Adv. Remote Sens.* **2016**, *5*, 28–42. [CrossRef]
73. Yue, J.; Yang, G.; Qi, X.; Wang, Y. Soil moisture retrieval in well covered farmland by Radarsat-2 SAR data. *Int. Geosci. Remote Sens. Symp.* **2016**, *3*, 1699–1702.
74. Beriaux, E.; Lucau-Danila, C.; Auquiere, E.; Defourny, P. Multiyear independent validation of the water cloud model for retrieving maize leaf area index from SAR time series. *Int. J. Remote Sens.* **2013**, *34*, 4156–4181. [CrossRef]
75. Srivastava, H.S.; Patel, P.; Sharma, Y.; Navalgund, R.R. Multi-frequency and multi-polarized SAR response to thin vegetation and scattered trees. *Curr. Sci.* **2009**, *97*, 425–429.